Aberrant expression profiles and bioinformatic analysis of CAF-derived exosomal miRNAs from three moderately differentiated supraglottic LSCC patients

Chunping Wu
Fudan University Eye Ear Nose and Throat Hospital
Mei Wang
Shanghai Municipal hospital of Traditional Chinese Medicine
Qiang Huang
Fudan University Eye Ear Nose and Throat Hospital
Yang Guo
Fudan University Eye Ear Nose and Throat Hospital
Hongli Gong
Fudan University Eye Ear Nose and Throat Hospital
Chunyan Hu
Fudan University Eye Ear Nose and Throat Hospital
Liang Zhou (zhoulent@163.com)
Fudan University Eye Ear Nose and Throat Hospital

Research

Keywords: Exosome, MiRNAs, Cancer-associated fibroblast, Supraglottic, laryngeal squamous cell carcinoma

Posted Date: June 10th, 2020

DOI: https://doi.org/10.21203/rs.3.rs-34245/v1

Version of Record: A version of this preprint was published at Journal of Clinical Laboratory Analysis on November 17th, 2021. See the published version at https://doi.org/10.1002/jcla.24108.

Abstract

Background

Aberrant expression of exosomal miRNAs has emerged as a research hotspot in cancer studies. However, no studies have been conducted on the dysregulation of exosomal miRNAs derived from cancer-associated fibroblasts (CAFs) in supraglottic laryngeal squamous cell carcinoma (SLSCC).

Methods

CAFs and paired normal fibroblasts (NFs) from SLSCC patients were cultured, and exosomes in the culture supernatants were collected and identified by transmission electron microscopy, nanoparticle tracking analysis and western blotting. Exosomal miRNA expression was compared in each pair of CAFs and NFs by next-generation sequencing. Four online bioinformatic algorithms predicted the potential target genes of aberrantly expressed miRNAs, while gene ontology and Kyoto Encyclopaedia of Genes and Genomes (KEGG) pathway enrichment and network analysis identified downstream target genes and their interactions.

Results

Three pairs of CAFs and NFs were successfully cultured and purified. CAF-derived exosomal miRNAs were mostly downregulated and included miR-656-3p, miR-337-5p, miR-29a-3p and miR-655-3p; however, some, including miR-184-3p, miR-92a-1-5p, miR-212-3p and miR-3135b, were upregulated. Bioinformatics analysis revealed involvement of these miRNAs in biological processes, cellular components and molecular functions. KEGG analysis revealed the top thirty pathways involvement in cancer initiation and progression and in cell cycle regulation. An interaction network showed miR-16-5p, miR-29a-3p, miR-34c-5p, miR-32-5p and miR-490-5p as the top five miRNAs and CCND1, CDKN1B, CDK6, PTEN and FOS as the top five target genes.

Conclusions

SLSCC patients showed aberrant expression of CAF-derived exosomal miRNAs. The target genes may jointly constitute a carcinogenic tumour microenvironment and may play decisive roles in the initiation and progression of SLSCC.

Background

Supraglottic laryngeal squamous cell carcinoma (SLSCC) is a special type of laryngeal cancer that is prone to lymph node metastasis and post-therapeutic relapse [1]. Tumour relapse is mainly caused by a disordered tumour microenvironment (TME) [2, 3], caused in part by the pro-tumourigenic capacity of

cancer-associated fibroblasts (CAFs), one of the most abundant stromal cell types in the TME [4, 5]. CAFs produce extensive exosomes—extracellular vesicles with diameters ranging from 30 to 100 nm—that regulate the TME and direct the growth and progression of cancer cells [6, 7].

Exosomes carry a variety of bioactive molecules, including miRNAs, signal peptides, lipids and DNA [8]. Of these molecules, the exosomal miRNAs play an important role in the modulation of the TME, and the aberrant expression of the exosome-derived miRNAs in CAFs are recognized as important contributors to cancer progression, metastasis and therapeutic resistance in different solid tumours [9]. The pro-tumourigenic potential of CAF-derived exosomal miRNAs has been validated by several recent studies [6, 10–12]. However, to date, no studies have been conducted to explore the aberrant expression profiles of CAF-derived exosomal miRNAs in patients with SLSCC.

In the present study, we compared exosomal miRNAs from pairs of CAFs and normal fibroblasts (NFs) to identify the aberrant expression profiles of CAF-derived exosomal miRNAs obtained from different patients with SLSCC. We then characterized the associated target genes and used bioinformatics analysis to identify vital signalling pathways. A few similar studies have been reported previously, but those studies focused on only a single pair of CAFs and NFs. For more reliable data, we collected ten pairs of SLSCC and normal connective tissue specimens for culture. However, only three pairs were successfully cultured and purified due to contamination or poor propagation capacity of NFs in vitro. The aberrant expression profiles of exosomal miRNAs from the three pairs of CAFs and NFs were identified using next-generation sequencing.

Most of the dysregulated exosomal miRNAs were downregulated, including miR-656-3p, miR-337-5p, miR-29a-3p, miR-655-3p, miR-16-5p, miR-34c-5p, miR-32-5p and miR-490-5p. A few dysregulated exosomal miRNAs were upregulated, including miR-184-3p, miR-92a-1-5p, miR-212-3p, miR-3135b, miR-1306-3p, miR-7704 and miR-1306-3p. The potential downstream target genes and their interactions with these selected exosomal miRNAs were explored by online bioinformatics analysis. Taken together, our findings indicate that these aberrantly expressed exosomal miRNAs, their target genes and the related vital signalling pathways may play critical roles in SLSCC initiation and progression and may provide new insights for the treatment of SLSCC.

Methods

Patient information

Ten tumour specimens from ten male patients with SLSCC diagnosed by biopsy and pathology were collected immediately after surgical tumour resection. All ten specimens were classified as moderately differentiated epiglottic LSCC. Paired adjacent normal connective tissues were obtained simultaneously from each patient. Data including laryngoscopic photos, contrast-enhanced computed tomography (CT) scans and pathologic photos were also collected.

Primary culture of tumour specimens and paired adjacent connective tissues

Each SLSCC specimen collected from fresh resected tumours was immersed immediately in cold RPMI 1640 medium (Invitrogen, Grand Island, NY, USA). The specimen was then immersed in povidone-iodine solution (saline-diluted, 1:10, 5 min), followed by gentamycin sulphate solution (saline-diluted, 1:8, 5 min) and finally lincomycin hydrochloride solution (saline-diluted, 1:8, 5 min). The specimen was then washed with phosphate-buffered saline (PBS) and scissored into fragments (1–2 mm^3). The fragments were trypsinised in RPMI 1640 medium containing type IV collagenase (200 U/mL, Sigma, St. Louis, MO, USA) for 12 h at 37 ℃. The digested fragments were suspended in bronchial epithelial cell growth medium (BEGM; Catalogue #CC-3170; Lonza, Walkersville, MD, USA) supplemented with 1% penicillin/streptomycin and 10% foetal bovine serum (FBS; Gibco, Life Technologies Corporation, Grand Island, NY, USA). The suspension was plated in 6 cm Petri dishes (Corning Inc., Corning, NY, USA) and incubated for 3–7 days in a humidified incubator in 5% CO_2 at 37℃. The dishes were then examined under a phase-contrast microscope and any contaminated dishes were discarded. The CAFs that grew successfully without contamination were collected and subcultured.

The paired adjacent connective tissue from the same patient was cultured using this same procedure and served as a control. Primary CAF and NF cultures were successfully generated from tissues from three of the ten patients.

Morphological examination and immunocytochemical staining of CAFs and NFs

CAFs and NFs were separated and purified by brief exposure to 0.25% trypsin-EDTA (Invitrogen, Grand Island, NY, USA). Representative images were recorded using a phase-contrast microscope. Immunocytochemistry was used to verify the identities of CAFs and NFs. The CAFs and NFs cells suspended in BEGM were plated on glass coverslips. The cells were then incubated at 37 ℃ for 24 h and immersed in 4% paraformaldehyde (PFA) for 15 min, washed with PBS, and incubated in 10% normal goat serum (Boster, Wuhan, China) for 40 min to block nonspecific interactions, in the presence or absence of 0.3% Triton X-100 to permeabilise the cells. The coverslips were immersed in solutions containing primary antibodies (rabbit antihuman) for pan-cytokeratin (CK; 1:400; Abcam, Cambridge, UK), vimentin (1:200; Abcam), α-smooth muscle actin (α-SMA; 1:200; Abcam) and fibroblast activation protein (FAP; 1:250; Abcam) and incubated at 4 ℃ overnight. The cells were then treated with secondary antibodies (Jackson ImmunoResearch, West Grove, PA, USA), either fluorescein isothiocyanate (FITC)-conjugated goat anti-rabbit IgG (H + L; 1:100) or $Cy^{TM}3$- conjugated goat anti-rabbit IgG (1:100) for 1 h at 37 ℃. The cell nuclei were stained with 4',6-diamidino-2-phenylindole (DAPI; Boster).

Collection of culture supernatant and isolation of exosomes

Purified CAFs and NFs were cultured in BEGM medium (containing 10% exosome-depleted FBS) for 72 h. When each cell monolayer was near confluence, the culture supernatant was collected and centrifuged (1500 *g*, 10 min), followed by centrifugation (10,000 *g*, 30 min) at 4˚C. The resulting exosome supernatant was then filtered (0.22 μm filter) to eliminate cellular debris, followed by centrifugal ultrafiltration (Amicon® Ultra-15 100 KDa; Merck KGaA) to prevent potential contamination. Exosomes were isolated from the ultrafiltered supernatant with Ribo™ Exosome Isolation Reagent (RiboBio Co., Ltd., Guangzhou, China), as previously described [13]. Briefly, the collected conditioned medium was mixed with Ribo™ Exosome Isolation Reagent (ratio 3:1), followed by an incubation at 4˚C overnight. The medium was then centrifuged (1500 *g*, 30 min) and the resulting exosome pellets were suspended in phosphate-buffered saline (PBS; HyClone; GE Healthcare Life Sciences) and analysed immediately or stored at -80˚C for subsequent research.

Transmission electron microscopy (TEM) and nanoparticle tracking analysis (NTA)

TEM was used to identify the morphological characteristics of exosome pellets, as described previously [13]. About 20 μL of exosome-PBS solution was added to carbon-coated copper grids for 1 min and then the excess solution was removed by blotting with filter paper. The exosome pellets were then stained with 20 μL uranyl acetate dihydrate (2%) for about 1 min. The sample was finally dried for 10 min under a lamp before observation with an FEI Tecnai G2 Spirit transmission electron microscope (FEI Company, Hillsboro, OR, USA) operated at 80 kV. The particle size distribution was determined by NTA using a NanoSight NS300 instrument (Malvern Instruments, Inc., Westborough, MA, USA), in accordance with the operating instructions.

Western blotting

Cell pellets and exosomes were lysed in RIPA lysis buffer. The protein concentration was determined, and protein samples from exosomes and control cells were separated by SDS polyacrylamide gel electrophoresis, followed by transfer to PVDF membranes (Millipore, Billerica, MA, USA). The membranes were initially blocked with 5% nonfat milk and probed overnight with rabbit primary anti-CD63 (1:1000, Abcam), anti-TSG101 (1:2000, Abcam) and anti-Calnexin (1:2000, Invitrogen), followed by detection using horseradish peroxidase-conjugated goat anti-mouse/rabbit/rat IgG (1:2,000; Jackson, Lancaster, PA, USA). Immunoreactive bands were detected using BeyoECL Plus (Beyotime Biotech, Nantong, China). Beta-actin antibody (1:5,000; HuaAn Biotech, Hangzhou, China) was used to normalise the amount of sample loaded.

Extraction of total RNA

TRIzol reagent (Invitrogen; Thermo Fisher Scientific, Inc., Waltham, MA, USA) was used to extract high-quality total RNA from the exosomes obtained from each specimen. A NanoDrop 2000 spectrophotometer (NanoDrop Technologies; Thermo Fisher Scientific, Inc.) was used to analyse the concentration and quality of RNA. An Agilent 2200 Bioanalyser (Agilent Technologies, Inc., Santa Clara, CA, USA) was used to assess the RNA content.

Small RNA (sRNA) sequencing

The sRNA next-generation sequencing technology was used to investigate differences in the miRNA profiles between exosomes from the three pairs of CAFs and NFs. The sRNA library preparation and sample sequencing were performed with the assistance of RiboBio Co., Ltd. (Guangzhou, China) using an Illumina HiSeq™ 2500 device, as described previously [13]. Briefly, total RNA from the three pairs of CAF and NF exosomes were concatenated with 5'- and 3'-adaptors, followed by cDNA synthesis and PCR amplification. The cDNA library (18–40 nt) was then obtained by acrylamide gel purification and single end (SE) sequencing was conducted (1 × 50 bp).

Identification of candidate exosomal miRNAs and target genes

The miRNAs that showed significant differences ($P<0.05$) between CAFs and NFs were selected as candidate exosomal miRNAs for further analysis. The genes targeted by selective exosomal miRNAs were predicted by four online bioinformatic algorithms: TargetScan (http://www.targetscan.org/vert_72/), miRDB (http://mirdb.org), miRTarBase (http://mirtarbase.mbc.nctu.edu.tw/php/index.php) and miRWalk (http://mirwalk.umm.uni-heidelberg.de). We selected an intersection among the four databases as a filtering condition to improve the accuracy of gene prediction. Only genes predicted simultaneously by specific exosomal miRNAs within the four databases were selected as target genes of the candidate exosomal miRNAs.

Gene Ontology (GO) and Kyoto Encyclopaedia of Genes and Genomes (KEGG) analysis

The GO analysis (http://www.geneontology.org/) was used to predict the potential functions of the target genes of selected miRNAs, while the KEGG (http://www.genome.jp/) pathway enrichment analysis was performed to identify the predominant pathways based on the DAVID 6.7 online software (http://david.abcc.ncifcrf.gov/home.jsp). All GO terms and KEGG pathway enrichment analysis were analysed with a $P<0.05$ threshold of significance.

Results

Laryngoscopy, contrast-enhanced CT and pathology

Laryngoscopy revealed that all the three SLSCC tumours originated from the epiglottis and showed obvious enhancement in CT scans. Pathological examination showed that all tumours were moderately differentiated squamous cell carcinomas (Fig. 1a-i).

Primary culture, purification and morphology of CAFs and NFs

Although ten pairs of CAFs and NFs from ten SLSCC patients were initially subjected to primary culture, only three pairs were successfully cultured and purified due to contamination or poor propagation of the NFs in vitro. Two days after seeding, the CAFs, cancer cells and NFs grew out from the fragments. The CAFs and NFs were purified by differential trypsinisation at passages 3–4. Purified CAFs and NFs were stored in liquid nitrogen. The morphology of the NFs showed small differences when compared with the CAFs. For example, fewer cell prominences were formed by the NFs than by the CAFs (Fig. 2a-h). During subculture, the proliferation capacity of CAFs and NFs did not decrease significantly within 7 consecutive passages. Therefore, CAFs and NFs between passages 3 and 6 were used for subsequent assays.

Purity and identification of CAFs and NFs by immunofluorescence

Negative staining for pan-CK and positive staining for vimentin were detected in CAFs and NFs, confirming their fibroblast origin. The purity of CAFs and NFs revealed by vimentin staining was 100%, as validated by examining 10 randomly selected microscopic fields (×200). In comparison with the NFs, CAFs also showed positive staining for FAP and α-SMA, two CAF biomarkers (Fig. 2i-r).

Isolation and identification of exosomes derived from CAFs and NFs

Exosomes were verified by TEM, western blotting and NTA. TEM images showed the typical size range and morphology of membrane-bound exosome particles, which were homogeneous in appearance (Fig. 2s). Western blotting revealed positive expression of CD63 and TSG101, two of the well-established surface markers for exosomes, and negative expression of calnexin, commonly used as a negative control for extracellular vesicles [14, 15] (Fig. 2t). In addition, NTA analysis showed a size distribution (mean diameter at 109.1 ± 44.1nm) for the exosome particles that was consistent with the reported size range of exosomes (30–150 nm) [16] (Fig. 2u).

Different small RNA signatures of the exosome compartments derived from CAFs and NFs

High-throughput sequencing was performed using RNA samples extracted from exosomes derived from the three pairs of CAFs and NFs. Most of the exosomal clean reads could be mapped to known RNAs of the human genome, as illustrated in the circos plots (Fig. 3). Analysis of the chromosomal location of all the mapped small RNAs indicated that they mainly originated from chromosomes 3, 5, 6, 7, 13 and 14. No significant differences were noted between CAFs and NFs for the distribution of the exosomal small RNA location in the genome (Fig. 3a). Approximately 12.3% of the miRNAs were common between CAFs-derived and NFs-derived exosomes (Fig. 3b). The small RNA reads were functionally categorised based on a >90% identity to exonic regions of the genome and annotated ncRNAs. Briefly, the miRNAs were the most abundant among the known sequences, followed by tRNAs, rRNA, snRNAs, snoRNA, Y RNAs, piRNAs and other RNAs that could not be categorised. Of all the small RNAs sequenced, an average of 67.61% of the miRNAs were detected in CAF-derived exosomes, compared with an average of 62.50% of the miRNAs in NF-derived exosomes (Fig. 3c). Small RNAs, sized between 17 nt and 45 nt, were analysed. Most of the sequenced small RNAs were approximately 20 nt and 31 nt in size (clean reads). These characteristic sizes were consistent with small RNA populations (Fig. 3d).

Aberrant expression profiles of exosomal miRNAs between CAFs and NFs

The sRNA next-generation sequencing technology was used in this assay. Total RNA was extracted from three pairs of CAF and NF exosomes. A small RNA library was prepared and samples were sequenced. Patient YYX had 668 dysregulated miRNAs; however, only 45 miRNAs showed significant differences in expression. Of those, 3 (hsa-miR-184, hsa-miR-92a-1-5p and hsa-miR-212-3p) were upregulated and 42 were downregulated ($P<0.05$, Table 1). Patient XHG had 576 dysregulated miRNAs, but only 45 miRNAs showed significant differences in expression. Of those, 9 (hsa-miR-184, hsa-miR-3135b, hsa-miR-7704, hsa-miR-485-3p, hsa-miR-365a-5p, hsa-miR-1248, hsa-miR-342-5p, hsa-miR-370-5p and hsa-miR-550a-3-5p) were upregulated and 36 were downregulated ($P<0.05$, Table 2). Patient YSX had 476 dysregulated miRNAs, but only 33 miRNAs showed significant differences in expression. Of those, 8 (hsa-miR-92a-1-5p, hsa-miR-1306-3p, hsa-miR-205-5p, hsa-miR-200b-5p, hsa-miR-615-3p, hsa-miR-4448, hsa-miR-223-5p and hsa-miR-412-5p) were upregulated and 25 were downregulated ($P<0.05$, Table 3) (Fig. 4). Eleven miRNAs (miR-452-5p, miR-651-5p, miR-16-5p, miR-424-5p, miR-378d, miR-32-5p, let-7i-3p, miR-16-2-3p, miR-136-3p, miR-221-5p, miR-34c-5p) were downregulated simultaneously in two patients. Two miRNAs (miR-184, miR-92a-1-5p) were upregulated simultaneously in two patients. Four miRNAs (miR-656-3p, miR-655-3p, miR-337-5p, miR-29a-3p) were downregulated simultaneously in all the three patients (Fig. 5a, pie chart).

Prediction of miRNAs target genes and GO and KEGG pathway enrichment analysis

The target gene prediction analysis of differentially expressed miRNAs between CAF-derived and NF-derived exosomes was performed using the TargetScan, miRDB, miRWalk and miRTarBase online

databases. Only the genes predicted simultaneously by all four servers were considered target genes of a specific miRNA.

The GO approach used to explore potential gene functions revealed that all the GO terms were involved in three categories: biological process, cellular component and molecular function. The top three biological processes (the lowest P-value, $P<0.05$) were related to regulation of transcription from the RNA polymerase II promoter, transcription from the RNA polymerase II promoter and positive regulation of RNA metabolic processes. The top three cellular components (the lowest P-value, $P<0.05$) were related to the RISC-loading complex, the micro-ribonucleoprotein complex and the RNAi effector complex. The top three molecular functions (the lowest P-value, $P<0.05$) were related to core promoter binding, regulatory region nucleic acid binding transcription factor activity and transcription regulatory region DNA binding (Fig. 5b-d, Fig.6a).

The KEGG pathway enrichment analysis was performed to characterise the predominant pathways. The specific miRNA targets were compared to the whole reference gene background, and $P<0.05$ was chosen as the cut-off criterion. Thirty signalling pathways with the most statistical differences were selected and analysed (Fig. 6b). These 30 pathways were involved in many types of cancers (non-small cell lung cancer, endometrial cancer, renal cell carcinoma, chronic myeloid leukemia, melanoma, colorectal cancer, pancreatic cancer, glioma, small cell lung cancer), several signalling pathways critical for cancer (the MAPK, mTOR, ErbB, Ras, p53, PI3K-Akt and FoxO signalling pathways), the cell cycle, miRNAs in cancer, signalling pathways regulating the pluripotency of stem cells and other cancer-related molecular functions (focal adhesion, adherens junctions and EGFR tyrosine kinase inhibitor resistance).

Interaction networks of exosomal miRNAs and target genes

One miRNA can regulate hundreds of target genes, and one gene can be regulated by multiple miRNAs. An interaction network of selected exosomal miRNAs and genes were constructed. In all, 12 aberrantly expressed exosomal miRNAs were identified that formed a wide range of connections with the corresponding target genes. The top five were miR-16-5p, miR-29a-3p, miR-34c-5p, miR-32-5p and miR-490-5p (Fig. 7a). The top five most common overlay genes were identified as CCND1 (gene count 10), CDKN1B (gene count 7), CDK6 (gene count 6), PTEN (gene count 5) and FOS (gene count 5) (Fig. 7b, Table 4).

Discussion

Increasing evidence reveals that dysregulation of exosomal miRNAs in the TME plays a critical role in cancer initiation, proliferation, vascularisation and metastasis, as well as other biological characteristics [17, 18]. Exosomal miRNAs may be derived from cancer cells themselves or from stromal cells like CAFs. To date, most studies have focused on exosomal miRNAs derived from cancer cells [19, 20]. CAF-derived

exosomal miRNAs are now receiving increasing attention, but no studies have yet been conducted to explore the aberrant expression profiles of exosomal miRNAs derived from CAFs in patients with SLSCC.

The present study is the first to describe dysregulation of the expression profile of miRNAs encapsulated in the CAF-derived exosomes in different patients with SLSCC and analysis of the potential involvement of their signalling cascade in cancer progression. Previous investigations have focused on only a single pair of CAFs and NFs, whereas we initially collected ten pairs of SLSCC specimens and paired normal connective tissues for primary culture. Three pairs were successfully cultured and used for subsequent investigations. Laryngoscopy revealed that all three SLSCC tumours originated from the epiglottis, with obvious enhancement in CT scans. Pathological examination showed that they were all moderately differentiated squamous cell carcinomas (Fig. 1a-i).

Both the CAFs and NFs showed long, fusiform morphology, with several cell prominences. However, the cell prominences were fewer on the NFs than on the CAFs, which probably reflected the fact that they were in a relatively inactive state (Fig. 2a-h). After purification, the CAFs were distinguished from the NFs by positive immunofluorescence staining for FAP and α-SMA, two CAFs biomarkers, indicating their activated state (Fig. 2i-r).

Exosomes, as intraluminal vesicles, range in size from 30 to 150 nm and can be isolated by various methods, such as ultracentrifugation, chromatography, density gradient separation and immunoaffinity capture techniques [21, 22]. In the present study, exosomes were isolated from conditioned media surrounding the CAFs and NFs using Ribo™ Exosome Isolation Reagent, as previously described [13].

The collected exosomes were verified as such by TEM, western blotting and NTA. TEM showed the typical size and morphology of membrane-bound exosome particles (Fig. 2s). Previous studies have reported that exosomes are generally enriched with certain specific marker proteins, such as CD9, CD63, CD81, TSG101 and HSP70 [23, 24], with lower expression of some cellular proteins, such as cis-Golgi matrix protein GM130 [25] and endoplasmic reticulum (ER) calnexin [14, 15]. Exosomes can therefore be identified by western blotting or flow cytometry. In the present study, we selected CD63 and TSG101 (two of the well-established surface markers for exosomes) and calnexin (a negative marker of extracellular vesicles) to confirm the isolation of exosomes by western blotting. The blots revealed the presence of CD63 and TSG101and the absence of calnexin, consistent with the previously reported characteristics of exosomes markers (Fig. 2t). In addition, NTA analysis showed the exosome particles to have a size of 109 ± 44.1 nm, which was consistent with the reported size range of exosomes (30–150 nm) [26] (Fig. 2u). Our findings confirmed that these isolated particles qualified as exosomes.

We also analysed the chromosomal locations and sequence lengths of the target small RNAs extracted from the exosomes derived from all three pairs of CAFs and NFs. We found that all the mapped small RNAs mainly originated from chromosomes 3, 5, 6, 7, 13 and 14. No significant difference was detected for the distribution of exosomal small RNAs locations in the genome between CAFs and NFs (Fig. 3a). Most sequenced small RNAs had a size of approximately 20 nt and 31 nt (clean reads), which was consistent with small RNA populations (Fig. 3d).

The aberrant expression profiles of exosomal miRNAs derived from the three pairs of purified CAFs and NFs from patients with SLSCC were then analysed by next-generation sequencing (Table 1–3, Fig. 4). Most of the aberrantly expressed miRNAs were downregulated, but a few were upregulated. Eleven miRNAs (miR-452-5p, miR-651-5p, miR-16-5p, miR-424-5p, miR-378d, miR-32-5p, let-7i-3p, miR-16-2-3p, miR-136-3p, miR-221-5p and miR-34c-5p) were downregulated simultaneously in two patients. Two miRNAs (miR-184 and miR-92a-1-5p) were upregulated simultaneously in two patients. Interestingly, four exosomal miRNAs (miR-656-3p, miR-655-3p, miR-337-5p and miR-29a-3p) were downregulated simultaneously in the purified CAFs from all three patients (Fig. 5a, pie chart).

A few reports have appeared about miR-656-3p and miR-337-5p and a few about miR-655-3p in different types of cancers. For example, miR-656-3p was found to be dysregulated in colon cancer tissues [27] and downregulated in non-small cell lung cancer tissues [28]. Overexpression of miR-337-5p in colorectal cancer tissues was significantly associated with improved overall survival [29]. Downregulation of miR-655-3p was reported in ovarian cancer tissues [30] and in hepatocellular carcinoma tissues and cell lines [31]. However, all three miRNAs in these reports were extracted either from tumour tissues or from cancer cell lines. None of the miRNAs were extracted from exosomes, let alone from the CAF-derived exosomes from different patients with SLSCC.

MiR-29a-3p is a potential tumour-suppressive miRNA and is downregulated in several cancer tissues, such as papillary thyroid carcinoma tissues and cell lines [32],hepatocellular carcinoma tissues and cell lines [33], gastric cancer tissues [34] and high-grade glioma tissues [35]. More studies have been conducted on miR-29a-3p than on miR-656-3p, miR-337-5p or miR-655-3p, and studies on exosome-derived miR-29a-3p are very rare. We found only one report that examined exosomal miR-29a-3p from oral squamous cell carcinoma cell lines [36]. No studies have reported CAF-derived exosomal miR-29a-3p.

Eleven miRNAs (miR-452-5p, miR-651-5p, miR-16-5p, miR-424-5p, miR-378d, miR-32-5p, let-7i-3p, miR-16-2-3p, miR-136-3p, miR-221-5p and miR-34c-5p) were downregulated simultaneously in two patients. However, the results in previous reports were controversial. The expression of miR-452-5p was significantly increased in 387 clinical lung squamous cell carcinoma specimens [37] and renal cell carcinoma tissues [38], whereas it was downregulated in 1007 prostate cancer samples [39]. MiR-16-5p has been proposed to function as a tumour suppressor and it was downregulated in non-small cell lung cancer cell lines [40], breast cancer samples [41], hepatocellular carcinoma tissues [42], chordoma tissues [43] and glioma tissues [44]. It was also downregulated in the plasma of gastric cancer patients [45]. However, exosomal miR-16-5p was upregulated in malignant mesothelioma cell lines [46]. The expression of miR-424-5p was significantly decreased in liver cancer tissues [47], intrahepatic cholangiocarcinoma tissues [48] and basal-like breast cancer tissues and cell lines [49]. However, it was upregulated in laryngeal squamous cell carcinoma tissues [50], thyroid cancer tissues [51], gastric cancer tissues and cells [52] and oesophageal squamous cell carcinoma tissues and cell lines [53]. A significant downregulation of miR-32-5p was reported in cervical cancer tissues and cells [54], but a significantly upregulation was detected in colorectal cancer tissues [55] and prostate cancer tissues and cells [56]. MiR-34c-5p was downregulated in leukaemia stem cells [57], osteosarcoma tissues and cells [58] and

aryngeal squamous cell carcinoma [59]. Let-7i-3p was upregulated in the serum-derived exosomes from osteosarcoma patients [60], but downregulated in the sera of lung cancer patients [61] and in hepatoblastoma tumours [62]. MiR-16-2-3p was downregulated in locally advanced gastric cancer samples [63] and upregulated in sera of patients with pancreatic ductal adenocarcinoma [64].MiR-221-5p was significantly upregulated in renal cell carcinoma tissues and cell lines [65], but downregulated in prostate cancer samples [66]. No studies have reported the regulation of miR-651-5p, miR-378d and miR-136-3p in cancer research.

The two miRNAs (miR-184, miR-92a-1-5p) that were upregulated simultaneously in two patients in our study have also had controversial findings. For example, miR-184 expression was upregulated in tongue squamous cell carcinoma tissues and cell lines [67, 68], hepatocellular carcinoma tissues [69] and renal carcinoma tissues [70], but it was downregulated in glioblastoma tissues and cell lines [71], nasopharyngeal carcinoma cell lines [72] and endometrial carcinoma tissues [73]. MiR-92a-1-5p was upregulated in tumours from the luminal A to the basal-like prostate cancer subtypes [74] but downregulated in urinary exosomes from prostate cancer patients [75]. These results suggest that these miRNAs play different regulatory roles in different types of tumours.

However, most of the miRNAs reported in different studies were extracted from either tumour tissues or cancer cell lines. Most of the exosmal miRNAs reported in different studies were conducted using miRNAs extracted from cancer cell-derived exosomes. Although increasing studies focused on the exosmal miRNAs extracted from CAFs, almost all of them used only one pair of CAFs and NFs. And almost no of them were conducted using miRNAs extracted from exosomes derived from CAF primary cultures from different patients. We believe that the miRNAs with the most significant statistical difference or showing the same expression trends in more than one patient sample are the miRNAs that jointly constitute a carcinogenic TME and play decisive roles in the initiation and progression of SLSCC.

The bioinformatics analysis using four online databases (TargetScan, miRDB, miRWalk and miRTarBase) predicted the potential target genes of the exosome miRNAs that were differentially expressed between CAFs and NFs. Our exploration of the potential functions of these target genes using GO analysis revealed an involvement of three GO categories (biological process, cellular component and molecular function) that had transcription and regulation of RNA as important functions (Fig. 5b-d, Fig. 6a). The KEGG pathway enrichment analysis identified the top thirty pathways involved in many types of cancers, in critical signalling pathways in cancer initiation and progression and in regulation of the cell cycle. Our findings indicated that the differentially expressed exosomal miRNAs play a critical role in the processes of tumourigenesis and in the regulation of cancer-associated signalling pathways, the cell cycle and other aspects of cancer biology (Fig. 6b).

We also constructed an interaction network of selected exosomal miRNAs and target genes. This network contained 12 aberrantly expressed exosomal miRNAs that formed a wide range of connections with the corresponding target genes (Fig. 7a). Of these, the top five miRNAs were miR-16-5p, miR-29a-3p, miR-34c-5p, miR-32-5p and miR-490-5p. MiR-16-5p was reportedly downregulated in breast cancer [76],

hepatocellular carcinoma [77] and glioma [78], in agreement with our findings. Overall, miR-29a-3p has been reported to function as a tumour suppressor and is downregulated in many types of cancers, such as thyroid carcinoma [32], colorectal carcinoma [79] and hepatocellular carcinoma [80].The downregulation of miR-34c-5p has been reported in several types of cancer, such as leukaemia [57] and osteosarcoma [58], and it has been closely associated with poor prognosis. Similarly, miR-490-5p is markedly downregulated in hepatocellular carcinoma tissues [81], in renal cell carcinoma tissues and cells [82] and in childhood neuroblastomas and cell lines [83]. MiR-32-5p was significantly downregulated in cervical cancer tissues and cells [54] but significantly upregulated in colorectal cancer tissues [55]. In our study, the expression of exosomal miR-32-5p was significantly repressed in CAFs compared to NFs, indicating that miR-32-5p might play different regulatory roles in different cancers.

We also found the top five most common overlay target genes (CCND1, CDKN1B, CDK6, PTEN and FOS) (Fig. 7b, Table 4). Of these, CCND1, CDKN1B and CDK6 are critical regulatory subunits required for the cell cycle G1/S transition. Cancer cells frequently overcome pRb-dependent growth inhibition by phosphorylation thereby inactivating pRb function by cyclin-dependent kinase (CDK) partnered with cyclin D, termed cyclin-CDK complexes. The CDKN1B gene that encodes for the p27 protein, acts as a cyclin dependent kinase (CDK) inhibitor. Dysfunction of these three genes may therefore lead to uncontrolled cell cycle progression and ultimately to tumourigenesis [84, 85].

PTEN acts as an inactivated tumour suppressor gene in cancer. It is a critical negative regulator of the PI3K signalling pathway, which is one of the most significant cell growth and survival signalling pathways in cancer. Variation in or loss of the PTEN gene is commonly observed in many types of human cancers. PTEN inhibits tumourigenesis through different mechanisms, such as phosphatase-dependent and independent activities that modulate a variety of cellular functions including DNA repair, growth, proliferation and cell motility [86, 87]. The Fos gene family (c-Fos, FosB, Fra-1 and Fra-2) dimerise with Jun proteins to form the transcription factor complex AP-1. Genes regulated by AP-1 include important regulators of proliferation, differentiation, invasion, metastasis, hypoxia and angiogenesis [88] and may play important roles in the initiation and progression of cancer.

Conclusions

Primary cultures were successfully obtained for three pairs of CAFs and NFs from ten SLSCC patients. The aberrant expression profile of CAF-derived exosomal miRNAs was then identified by next-generation sequencing. Important functions of the predicted target genes were revealed by bioinformatics analysis. The top thirty pathways involved in cancer initiation and progression and in cell cycle regulation were identified by KEGG analysis. The top five miRNAs, miR-16-5p, miR-29a-3p, miR-34c-5p, miR-32-5p and miR-490-5p, and the top five most common overlay target genes, CCND1, CDKN1B, CDK6, PTEN and FOS, were revealed by the interaction network. Our findings predict that these critical miRNAs and target genes may jointly constitute a carcinogenic TME and may play decisive roles in the initiation and progression of SLSCC. Therefore, they may represent promising candidate targets for therapeutic intervention. However, these predictions require further experimental exploration in future studies.

Abbreviations

CAFs: cancer-associated fibroblasts; SLSCC: supraglottic laryngeal squamous cell carcinoma; NFs: normal fibroblasts; TEM: transmission electron microscopy; NTA: nanoparticle tracking analysis; GO: Gene Ontology; KEGG: Kyoto Encyclopaedia of Genes and Genomes; TME: tumour microenvironment; CT: computed tomography; PBS: phosphate-buffered saline; BEGM: bronchial epithelial cell growth medium.

Declarations

Acknowledgments

We thank Dr. Zuopeng Lin in RiboBio Co., Ltd (Guangzhou, China) for his great help in bioinformatics analysis.

Author's contributions

Chunping Wu, Mei Wang and Liang Zhou conceived and designed the study. Chunping Wu, Qiang Huang and Chunyan Hu performed the experiments. Chunping Wu, Mei Wang, Yang Guo and Hongli Gong analysed the data. Chunping Wu and Mei Wang wrote the manuscript. Yang Guo, Hongli Gong and Liang Zhou reviewed and edited the manuscript. All authors read and approved the final manuscript.

Funding

This study was supported by grants from the National Natural Science Foundations of China (grant no. 81972529)

Availability of data and materials

All data generated or analysed during this study are available in this published article.

Ethics approval and consent to participate

All SLSCC specimens were obtained with the approval of the Ethics Committee of the Eye, Ear, Nose and Throat Hospital, Fudan University, Shanghai, China. Signed informed consents were obtained from all patients included in this study.

Consent for publication

All authors reached an agreement to publish the study in this journal.

Competing interests

The authors declare that they have no competing interests.

References

1. Patel TD, Echanique KA, Yip C, Hsueh WD, Baredes S, Park RCW, Eloy JA. Supraglottic Squamous Cell Carcinoma: A Population-Based Study of 22,675 Cases. Laryngoscope. 2019;129(8):1822–7.
2. Correia AL, Bissell MJ. The tumor microenvironment is a dominant force in multidrug resistance. Drug Resist Updat. 2012;15(1–2):39–49.
3. Casey SC, Amedei A, Aquilano K, Azmi AS, Benencia F, Bhakta D, Bilsland AE, Boosani CS, Chen S, Ciriolo MR, et al. Cancer prevention and therapy through the modulation of the tumor microenvironment. Semin Cancer Biol. 2015;35(Suppl(Suppl):199-s223.
4. Sidaway P. Breast cancer: Fibroblast subtypes alter the microenvironment. Nat Rev Clin Oncol. 2018;15(5):264–5.
5. Cully M. Tumour microenvironment: Fibroblast subtype provides niche for cancer stem cells. Nat Rev Cancer. 2018;18(3):136.
6. Hu JL, Wang W, Lan XL, Zeng ZC, Liang YS, Yan YR, Song FY, Wang FF, Zhu XH, Liao WJ, et al. CAFs secreted exosomes promote metastasis and chemotherapy resistance by enhancing cell stemness and epithelial-mesenchymal transition in colorectal cancer. Mol Cancer. 2019;18(1):91.
7. Luga V, Wrana JL. Tumor-stroma interaction: Revealing fibroblast-secreted exosomes as potent regulators of Wnt-planar cell polarity signaling in cancer metastasis. Cancer Res. 2013;73(23):6843–7.
8. Azmi AS, Bao B, Sarkar FH. Exosomes in cancer development, metastasis, and drug resistance: a comprehensive review. Cancer Metastasis Rev. 2013;32(3–4):623–42.
9. Yang F, Ning Z, Ma L, Liu W, Shao C, Shu Y, Shen H. Exosomal miRNAs and miRNA dysregulation in cancer-associated fibroblasts. Mol Cancer. 2017;16(1):148.
10. Xu G, Zhang B, Ye J, Cao S, Shi J, Zhao Y, Wang Y, Sang J, Yao Y, Guan W, et al. Exosomal miRNA-139 in cancer-associated fibroblasts inhibits gastric cancer progression by repressing MMP11 expression. Int J Biol Sci. 2019;15(11):2320–9.
11. Qin X, Guo H, Wang X, Zhu X, Yan M, Wang X, Xu Q, Shi J, Lu E, Chen W, et al. Exosomal miR-196a derived from cancer-associated fibroblasts confers cisplatin resistance in head and neck cancer through targeting CDKN1B and ING5. Genome Biol. 2019;20(1):12.
12. Wu HJ, Hao M, Yeo SK, Guan JL. FAK signaling in cancer-associated fibroblasts promotes breast cancer cell migration and metastasis by exosomal miRNAs-mediated intercellular communication. Oncogene. 2020;39(12):2539–49.
13. Huang Q, Yang J, Zheng J, Hsueh C, Guo Y, Zhou L. Characterization of selective exosomal microRNA expression profile derived from laryngeal squamous cell carcinoma detected by next generation sequencing. Oncol Rep. 2018;40(5):2584–94.
14. Lässer C, O'Neil SE, Ekerljung L, Ekström K, Sjöstrand M, Lötvall J. RNA-containing exosomes in human nasal secretions. Am J Rhinol Allergy. 2011;25(2):89–93.
15. Li X, Li X, Lin J, Sun X, Ding Q. Exosomes Derived From Low-Intensity Pulsed Ultrasound-Treated Dendritic Cells Suppress Tumor Necrosis Factor-Induced Endothelial Inflammation. J Ultrasound Med. 2019;38(8):2081–91.

16. Schageman J, Zeringer E, Li M, Barta T, Lea K, Gu J, Magdaleno S, Setterquist R, Vlassov AV. The complete exosome workflow solution: from isolation to characterization of RNA cargo. Biomed Res Int. 2013; 2013:253957.
17. Bhome R, Del Vecchio F, Lee G-H, Bullock MD, Primrose JN, Sayan AE, Mirnezami AH. Exosomal microRNAs (exomiRs): Small molecules with a big role in cancer. Cancer Lett. 2018;420:228–35.
18. Sun Z, Shi K, Yang S, Liu J, Zhou Q, Wang G, Song J, Li Z, Zhang Z, Yuan W. Effect of exosomal miRNA on cancer biology and clinical applications. Mol Cancer. 2018;17(1):147–7.
19. Wang M, Yu F, Ding H, Wang Y, Li P, Wang K. Emerging Function and Clinical Values of Exosomal MicroRNAs in Cancer. Mol Ther Nucleic Acids. 2019;16:791–804.
20. Sundararajan V, Sarkar FH, Ramasamy TS. The multifaceted role of exosomes in cancer progression: diagnostic and therapeutic implications [corrected]. Cell Oncol (Dordr). 2018;41(3):223–52.
21. Thery C, Zitvogel L, Amigorena S. Exosomes: composition, biogenesis and function. Nat Rev Immunol. 2002;2(8):569–79.
22. Coumans FAW, Brisson AR, Buzas EI, Dignat-George F, Drees EEE, El-Andaloussi S, Emanueli C, Gasecka A, Hendrix A, Hill AF, et al. Methodological Guidelines to Study Extracellular Vesicles. Circ Res. 2017;120(10):1632–48.
23. Zhang G, Chen L, Guo X, Wang H, Chen W, Wu G, Gu B, Miao W, Kong J, Jin X, et al. Comparative Analysis of microRNA Expression Profiles of Exosomes Derived from Normal and Hypoxic Preconditioning Human Neural Stem Cells by Next Generation Sequencing. J Biomed Nanotechnol. 2018;14(6):1075–89.
24. Zhang Z, Li X, Sun W, Yue S, Yang J, Li J, Ma B, Wang J, Yang X, Pu M, et al. Loss of exosomal miR-320a from cancer-associated fibroblasts contributes to HCC proliferation and metastasis. Cancer Lett. 2017;397:33–42.
25. Lotvall J, Hill AF, Hochberg F, Buzas EI, Di Vizio D, Gardiner C, Gho YS, Kurochkin IV, Mathivanan S, Quesenberry P, et al. Minimal experimental requirements for definition of extracellular vesicles and their functions: a position statement from the International Society for Extracellular Vesicles. J Extracell Vesicles. 2014;3:26913.
26. Zeringer E, Barta T, Li M, Vlassov AV. Strategies for isolation of exosomes. Cold Spring Harb Protoc. 2015; 2015(4):319–323.
27. Jacob H, Stanisavljevic L, Storli KE, Hestetun KE, Dahl O, Myklebust MP. A four-microRNA classifier as a novel prognostic marker for tumor recurrence in stage II colon cancer. Sci Rep. 2018;8(1):6157–7.
28. Chen T, Qin S, Gu Y, Pan H, Bian D. Long non-coding RNA NORAD promotes the occurrence and development of non-small cell lung cancer by adsorbing MiR-656-3p. Mol Genet Genomic Med. 2019;7(8):e757–7.
29. Molina-Pinelo S, Carnero A, Rivera F, Estevez-Garcia P, Bozada JM, Limon ML, Benavent M, Gomez J, Pastor MD, Chaves M, et al. MiR-107 and miR-99a-3p predict chemotherapy response in patients with advanced colorectal cancer. BMC Cancer. 2014;14:656–6.

30. Zha JF, Chen DX. MiR-655-3p inhibited proliferation and migration of ovarian cancer cells by targeting RAB1A. Eur Rev Med Pharmacol Sci. 2019;23(9):3627–34.
31. Wu G, Zheng K, Xia S, Wang Y, Meng X, Qin X, Cheng Y. MicroRNA-655-3p functions as a tumor suppressor by regulating ADAM10 and β-catenin pathway in Hepatocellular Carcinoma. J Exp Clin Cancer Res. 2016;35(1):89–9.
32. Ma Y, Sun Y. miR-29a-3p inhibits growth, proliferation, and invasion of papillary thyroid carcinoma by suppressing NF-κB signaling via direct targeting of OTUB2. Cancer Manag Res. 2018;11:13–23.
33. Xiao Z, Wang Y, Ding H. XPD suppresses cell proliferation and migration via miR-29a-3p-Mdm2/PDGF-B axis in HCC. Cell Biosci. 2019;9:6–6.
34. Zhao Z, Wang L, Song W, Cui H, Chen G, Qiao F, Hu J, Zhou R, Fan H. Reduced miR-29a-3p expression is linked to the cell proliferation and cell migration in gastric cancer. World J Surg Oncol. 2015;13:101–1.
35. Catanzaro G, Sabato C, Russo M, Rosa A, Abballe L, Besharat ZM, Po A, Miele E, Bellavia D, Chiacchiarini M, et al. Loss of miR-107, miR-181c and miR-29a-3p Promote Activation of Notch2 Signaling in Pediatric High-Grade Gliomas (pHGGs). Int J Mol Sci. 2017;18(12):2742.
36. Cai J, Qiao B, Gao N, Lin N, He W. Oral squamous cell carcinoma-derived exosomes promote M2 subtype macrophage polarization mediated by exosome-enclosed miR-29a-3p. Am J Physiol Cell Physiol. 2019;316(5):C731–40.
37. Gan XN, Gan TQ, He RQ, Luo J, Tang RX, Wang HL, Zhou H, Qing H, Ma J, Hu XH, et al. Clinical significance of high expression of miR-452-5p in lung squamous cell carcinoma. Oncol Lett. 2018;15(5):6418–30.
38. Zhai W, Li S, Zhang J, Chen Y, Ma J, Kong W, Gong D, Zheng J, Xue W, Xu Y. Sunitinib-suppressed miR-452-5p facilitates renal cancer cell invasion and metastasis through modulating SMAD4/SMAD7 signals. Mol Cancer. 2018;17(1):157.
39. Gao L, Zhang LJ, Li SH, Wei LL, Luo B, He RQ, Xia S. Role of miR-452-5p in the tumorigenesis of prostate cancer: A study based on the Cancer Genome Atl(TCGA), Gene Expression Omnibus (GEO), and bioinformatics analysis. Pathol Res Pract. 2018;214(5):732–49.
40. Wang Q, Chen Y, Lu H, Wang H, Feng H, Xu J, Zhang B. Quercetin radiosensitizes non-small cell lung cancer cells through the regulation of miR-16-5p/WEE1 axis. IUBMB Life. 2020;72(5):1012–22.
41. Ruan L, Qian X. MiR-16-5p inhibits breast cancer by reducing AKT3 to restrain NF-κB pathway. Biosci Rep. 2019; 39(8).
42. Cheng B, Ding F, Huang CY, Xiao H, Fei FY, Li J. Role of miR-16-5p in the proliferation and metastasis of hepatocellular carcinoma. Eur Rev Med Pharmacol Sci. 2019;23(1):137–45.
43. Zhang H, Yang K, Ren T, Huang Y, Tang X, Guo W. miR-16-5p inhibits chordoma cell proliferation, invasion and metastasis by targeting Smad3. Cell Death Dis. 2018;9(6):680.
44. Krell A, Wolter M, Stojcheva N, Hertler C, Liesenberg F, Zapatka M, Weller M, Malzkorn B, Reifenberger G. MiR-16-5p is frequently down-regulated in astrocytic gliomas and modulates glioma cell

proliferation, apoptosis and response to cytotoxic therapy. Neuropathol Appl Neurobiol. 2019;45(5):441–58.

45. Zhang J, Song Y, Zhang C, Zhi X, Fu H, Ma Y, Chen Y, Pan F, Wang K, Ni J, et al. Circulating MiR-16-5p and MiR-19b-3p as Two Novel Potential Biomarkers to Indicate Progression of Gastric Cancer. Theranostics. 2015;5(7):733–45.
46. Munson PB, Hall EM, Farina NH, Pass HI, Shukla A. Exosomal miR-16-5p as a target for malignant mesothelioma. Sci Rep. 2019;9(1):11688.
47. Piao L, Wang F, Wang Y, Yang Z, Li Q, Cui L, Yu Q. miR-424-5p Regulates Hepatoma Cell Proliferation and Apoptosis. Cancer Biother Radiopharm. 2019;34(3):196–202.
48. Wu J, Yang B, Zhang Y, Feng X, He B, Xie H, Zhou L, Wu J, Zheng S. miR-424-5p represses the metastasis and invasion of intrahepatic cholangiocarcinoma by targeting ARK5. Int J Biol Sci. 2019;15(8):1591–9.
49. Wang J, Wang S, Zhou J, Qian Q. miR-424-5p regulates cell proliferation, migration and invasion by targeting doublecortin-like kinase 1 in basal-like breast cancer. Biomed Pharmacother. 2018;102:147–52.
50. Li Y, Liu J, Hu W, Zhang Y, Sang J, Li H, Ma T, Bo Y, Bai T, Guo H, et al. miR-424-5p Promotes Proliferation, Migration and Invasion of Laryngeal Squamous Cell Carcinoma. Onco Targets Ther. 2019;12:10441–53.
51. Liu X, Fu Y, Zhang G, Zhang D, Liang N, Li F, Li C, Sui C, Jiang J, Lu H, et al. miR-424-5p Promotes Anoikis Resistance and Lung Metastasis by Inactivating Hippo Signaling in Thyroid Cancer. Mol Ther Oncolytics. 2019;15:248–60.
52. Wei S, Li Q, Li Z, Wang L, Zhang L, Xu Z. miR-424-5p promotes proliferation of gastric cancer by targeting Smad3 through TGF-β signaling pathway. Oncotarget. 2016;7(46):75185–96.
53. Wang F, Wang J, Yang X, Chen D, Wang L. MiR-424-5p participates in esophageal squamous cell carcinoma invasion and metastasis via SMAD7 pathway mediated EMT. Diagn Pathol. 2016;11(1):88.
54. Liu YJ, Zhou HG, Chen LH, Qu DC, Wang CJ, Xia ZY, Zheng JH. MiR-32-5p regulates the proliferation and metastasis of cervical cancer cells by targeting HOXB8. Eur Rev Med Pharmacol Sci. 2019;23(1):87–95.
55. Liang H, Tang Y, Zhang H, Zhang C. MiR-32-5p Regulates Radiosensitization, Migration And Invasion Of Colorectal Cancer Cells By Targeting TOB1 Gene. Onco Targets Ther. 2019;12:9651–61.
56. Gao ZQ, Wang JF, Chen DH, Ma XS, Wu Y, Tang Z, Dang XW. Long non-coding RNA GAS5 suppresses pancreatic cancer metastasis through modulating miR-32-5p/PTEN axis. Cell Biosci. 2017;7:66.
57. Peng D, Wang H, Li L, Ma X, Chen Y, Zhou H, Luo Y, Xiao Y, Liu L. miR-34c-5p promotes eradication of acute myeloid leukemia stem cells by inducing senescence through selective RAB27B targeting to inhibit exosome shedding. Leukemia. 2018;32(5):1180–8.
58. Wang Y, Wang X, Tang J, Su X, Miao Y. The study of mechanism of miR-34c-5p targeting FLOT2 to regulate proliferation, migration and invasion of osteosarcoma cells. Artif Cells Nanomed Biotechnol.

2019;47(1):3559–68.

59. Re M, Magliulo G, Gioacchini FM, Bajraktari A, Bertini A, Çeka A, Rubini C, Ferrante L, Procopio AD, Olivieri F. Expression Levels and Clinical Significance of miR-21-5p, miR-let-7a, and miR-34c-5p in Laryngeal Squamous Cell Carcinoma. Biomed Res Int. 2017; 2017:3921258.
60. Ye Z, Zheng Z, Peng L. MicroRNA profiling of serum exosomes in patients with osteosarcoma by high-throughput sequencing. J Investig Med. 2020;68(4):893–901.
61. Huang J, Wu J, Li Y, Li X, Yang T, Yang Q, Jiang Y. Deregulation of serum microRNA expression is associated with cigarette smoking and lung cancer. Biomed Res Int. 2014; 2014:364316.
62. Indersie E, Lesjean S, Hooks KB, Sagliocco F, Ernault T, Cairo S, Merched-Sauvage M, Rullier A, Le Bail B, Taque S, et al. MicroRNA therapy inhibits hepatoblastoma growth in vivo by targeting β-catenin and Wnt signaling. Hepatol Commmun. 2017;1(2):168–83.
63. Liu X, Cai H, Sheng W, Huang H, Long Z, Wang Y. microRNAs expression profile related with response to preoperative radiochemotherapy in patients with locally advanced gastric cancer. BMC Cancer. 2018;18(1):1048.
64. Su Q, Zhu EC, Qu YL, Wang DY, Qu WW, Zhang CG, Wu T, Gao ZH. Serum level of co-expressed hub miRNAs as diagnostic and prognostic biomarkers for pancreatic ductal adenocarcinoma. J Cancer. 2018;9(21):3991–9.
65. Liu S, Wang Y, Li W, Yu S, Wen Z, Chen Z, Lin F. miR-221-5p acts as an oncogene and predicts worse survival in patients of renal cell cancer. Biomed Pharmacother. 2019;119:109406.
66. Kiener M, Chen L, Krebs M, Grosjean J, Klima I, Kalogirou C, Riedmiller H, Kneitz B, Thalmann GN, Snaar-Jagalska E, et al. miR-221-5p regulates proliferation and migration in human prostate cancer cells and reduces tumor growth in vivo. BMC Cancer. 2019;19(1):627.
67. Chen D, Li J, Li S, Han P, Li N, Wang Y, Du S. miR-184 promotes cell proliferation in tongue squamous cell carcinoma by targeting SOX7. Oncol Lett. 2018;16(2):2221–8.
68. Wong TS, Liu XB, Wong BY, Ng RW, Yuen AP, Wei WI. Mature miR-184 as Potential Oncogenic microRNA of Squamous Cell Carcinoma of Tongue. Clin Cancer Res. 2008;14(9):2588–92.
69. Gao B, Gao K, Li L, Huang Z, Lin L. miR-184 functions as an oncogenic regulator in hepatocellular carcinoma (HCC). Biomed Pharmacother. 2014;68(2):143–8.
70. Yang J, Lai CC, Xian ZM, Wang WQ, Xu BL. Preliminary results indicate increased expression of miR-184 in patients with renal carcinoma. Eur Rev Med Pharmacol Sci. 2019;23(16):6878–87.
71. Feng L, Ma J, Ji H, Liu Y, Hu W. MiR-184 Retarded the Proliferation, Invasiveness and Migration of Glioblastoma Cells by Repressing Stanniocalcin-2. Pathol Oncol Res. 2018;24(4):853–60.
72. Zhu HM, Jiang XS, Li HZ, Qian LX, Du MY, Lu ZW, Wu J, Tian XK, Fei Q, He X, et al. miR-184 Inhibits Tumor Invasion, Migration and Metastasis in Nasopharyngeal Carcinoma by Targeting Notch2. Cell Physiol Biochem. 2018;49(4):1564–76.
73. Chen Z, Zhu Y, Fan X, Liu Y, Feng Q. Decreased expression of miR-184 restrains the growth and invasion of endometrial carcinoma cells through CDC25A-dependent Notch signaling pathway. Am J

Transl Res. 2019;11(2):755–64.

74. Oztemur Islakoglu Y, Noyan S, Aydos A, Gur Dedeoglu B. Meta-microRNA Biomarker Signatures to Classify Breast Cancer Subtypes. OMICS. 2018;22(11):709–16.
75. Rodríguez M, Bajo-Santos C, Hessvik NP, Lorenz S, Fromm B, Berge V, Sandvig K, Linē A, Llorente A. Identification of non-invasive miRNAs biomarkers for prostate cancer by deep sequencing analysis of urinary exosomes. Mol Cancer. 2017;16(1):156.
76. Ruan L, Qian X. MiR-16-5p inhibits breast cancer by reducing AKT3 to restrain NF-κB pathway. Biosci Rep. 2019;39(8):BSR20191611.
77. Cheng B, Ding F, Huang CY, Xiao H, Fei FY, Li J. Role of miR-16-5p in the proliferation and metastasis of hepatocellular carcinoma. Eur Rev Med Pharmacol Sci. 2019;23(1):137–45.
78. Krell A, Wolter M, Stojcheva N, Hertler C, Liesenberg F, Zapatka M, Weller M, Malzkorn B, Reifenberger G. MiR-16-5p is frequently down-regulated in astrocytic gliomas and modulates glioma cell proliferation, apoptosis and response to cytotoxic therapy. Neuropathol Appl Neurobiol. 2019;45(5):441–58.
79. Zheng Z, Cui H, Wang Y, Yao W. Downregulation of RPS15A by miR-29a-3p attenuates cell proliferation in colorectal carcinoma. Biosci Biotechnol Biochem. 2019;83(11):2057–64.
80. Wang X, Liu S, Cao L, Zhang T, Yue D, Wang L, Ping Y, He Q, Zhang C, Wang M, et al. miR-29a-3p suppresses cell proliferation and migration by downregulating IGF1R in hepatocellular carcinoma. Oncotarget. 2017;8(49):86592–603.
81. Yang H, Zhang L, Wang X-D, Huang M-L, Lin P, Pang Y-Y, Feng Z-B, Chen G. Potential targets and clinical value of miR-490-5p in hepatocellular carcinoma: a study based on TCGA, qRT-PCR and bioinformatics analyses. Int J Clin Exp Pathol. 2018;11(3):1123–34.
82. Chen K, Zeng J, Tang K, Xiao H, Hu J, Huang C, Yao W, Yu G, Xiao W, Guan W, et al. miR-490-5p suppresses tumour growth in renal cell carcinoma through targeting PIK3CA. Biol Cell. 2016;108(2):41–50.
83. Wang J, Zhang X, Yao H, Le Y, Zhou W, Li J, Lu L, Chen M, Li X. MiR-490-5p functions as tumor suppressor in childhood neuroblastoma by targeting MYEOV. Hum Cell. 2020;33(1):261–71.
84. VanArsdale T, Boshoff C, Arndt KT, Abraham RT. Molecular Pathways. Targeting the Cyclin D-CDK4/6 Axis for Cancer Treatment. Clin Cancer Res. 2015;21(13):2905–10.
85. Cusan M, Mungo G, De Marco Zompit M, Segatto I, Belletti B, Baldassarre G. Landscape of CDKN1B Mutations in Luminal Breast Cancer and Other Hormone-Driven Human Tumors. Front Endocrinol (Lausanne). 2018;9:393–3.
86. Milella M, Falcone I, Conciatori F, Cesta Incani U, Del Curatolo A, Inzerilli N, Nuzzo CMA, Vaccaro V, Vari S, Cognetti F, et al. PTEN: Multiple Functions in Human Malignant Tumors. Front Oncol. 2015;5:24–4.
87. Luongo F, Colonna F, Calapà F, Vitale S, Fiori ME, De Maria R. PTEN Tumor-Suppressor: The Dam of Stemness in Cancer. Cancers. 2019;11(8):1076.

88. Milde-Langosch K. The Fos family of transcription factors and their role in tumourigenesis. Eur J Cancer. 2005;41(16):2449–61.

Tables

Table 1. Dysregulated miRNAs of patient YYX

miRNA_ID	Up/Down (CAF/NF)	Log_2(fold change)	P Value
hsa-miR-184	up	1.3467	0.000436421
hsa-miR-1908-5p	down	-4.756	0.000461103
hsa-miR-2682-5p	down	-6.0463	0.000481147
hsa-miR-490-5p	down	-4.4747	0.000531751
hsa-miR-889-3p	down	-4.2412	0.000800056
hsa-miR-27a-3p	down	-4.0642	0.000847526
hsa-miR-651-5p	down	-5.2864	0.001005195
hsa-miR-500a-3p	down	-4.2237	0.001930205
hsa-miR-16-2-3p	down	-3.9804	0.002335581
hsa-miR-29a-3p	down	-3.7784	0.003350246
hsa-miR-452-5p	down	-4.6451	0.004046271
hsa-miR-655-3p	down	-4.5661	0.006131112
hsa-miR-549a	down	-3.604	0.008204082
hsa-miR-656-3p	down	-4.0266	0.009741014
hsa-miR-431-5p	down	-4.6448	0.011294317
hsa-miR-376c-3p	down	-5.2498	0.01143183
hsa-miR-199b-3p	down	-3.4461	0.01305138
hsa-miR-199a-3p	down	-3.4461	0.01305138
hsa-miR-92a-1-5p	up	2.5837	0.014078675
hsa-miR-27b-3p	down	-3.4062	0.015191207
hsa-miR-16-5p	down	-3.8592	0.015510297
hsa-miR-127-5p	down	-4.0889	0.017699623
hsa-miR-337-3p	down	-3.418	0.019501702
hsa-miR-212-3p	up	2.3208	0.021900161
hsa-miR-23a-3p	down	-3.2816	0.024944253
hsa-miR-24-2-5p	down	-3.426	0.025778677
hsa-miR-654-3p	down	-3.2898	0.026263483
hsa-miR-337-5p	down	-3.9787	0.026429163
hsa-miR-130a-3p	down	-3.4606	0.026655539
hsa-miR-502-3p	down	-3.3992	0.027379545
hsa-miR-136-3p	down	-3.2989	0.028788131
hsa-miR-148a-5p	down	-4.9088	0.029721761
hsa-miR-3679-5p	down	-3.9556	0.030291249
hsa-miR-22-3p	down	-3.2106	0.031760512
hsa-miR-221-5p	down	-3.2904	0.032286795
hsa-miR-143-3p	down	-3.2015	0.032767788
hsa-miR-323b-3p	down	-3.2233	0.032968318
hsa-miR-1180-3p	down	-3.2818	0.033582331

hsa-miR-490-3p	down	-4.0013	0.038005735
hsa-miR-665	down	-3.8594	0.03995467
hsa-miR-34c-5p	down	-3.509	0.041225225
hsa-miR-4326	down	-4.2489	0.042605988
hsa-miR-10b-3p	down	-3.3155	0.043362154
hsa-miR-433-3p	down	-3.1613	0.044973613
hsa-miR-24-3p	down	-3.0958	0.047595926

Table 2. Dysregulated miRNAs of patient XHG

miRNA_ID	Up/Down (CAF/NF)	Log_2(fold change)	P Value
hsa-miR-184	up	2.8747	2.74E-06
hsa-miR-10a-3p	down	-4.5591	9.22E-06
hsa-miR-424-5p	down	-5.7141	1.50E-05
hsa-miR-656-3p	down	-5.9762	0.000211308
hsa-miR-19b-3p	down	-5.9059	0.000291391
hsa-miR-3135b	up	1.085	0.000998657
hsa-miR-7704	up	1.3222	0.001325876
hsa-miR-485-3p	up	1.1231	0.001664599
hsa-miR-365a-5p	up	3.3231	0.001996045
hsa-miR-655-3p	down	-4.0874	0.002378747
hsa-miR-422a	down	-3.8579	0.002608669
hsa-miR-337-5p	down	-4.9532	0.004550577
hsa-miR-10a-5p	down	-3.129	0.004617302
hsa-miR-452-5p	down	-4.1695	0.005471847
hsa-miR-378f	down	-3.8073	0.007066228
hsa-miR-1248	up	2.8084	0.009223959
hsa-miR-30a-5p	down	-2.9311	0.010358919
hsa-miR-29a-3p	down	-2.8335	0.015686115
hsa-miR-342-5p	up	1.17	0.016272845
hsa-miR-421	down	-3.6626	0.016272845
hsa-miR-451a	down	-2.8371	0.016791706
hsa-miR-20a-5p	down	-2.8771	0.018607347
hsa-miR-483-3p	down	-2.9504	0.019050617
hsa-miR-651-5p	down	-4.0443	0.019112419
hsa-miR-296-3p	down	-2.9749	0.019201783
hsa-miR-7976	down	-4.4584	0.022208097
hsa-miR-378d	down	-2.8562	0.022272931
hsa-miR-32-5p	down	-3.5845	0.023710684
hsa-miR-542-3p	down	-3.2324	0.02695136
hsa-miR-329-3p	down	-2.745	0.028013799
hsa-miR-589-5p	down	-2.7465	0.02841603
hsa-miR-369-3p	down	-2.7002	0.030222401
hsa-miR-382-3p	down	-2.7933	0.030320537
hsa-miR-370-5p	up	2.3231	0.034782609
hsa-miR-374b-5p	down	-3.459	0.034945041
hsa-let-7a-3p	down	-2.6346	0.039630593
hsa-miR-378a-3p	down	-2.5784	0.039661431
hsa-let-7i-3p	down	-4.2469	0.039696281

hsa-miR-550a-3-5p	up	1.5854	0.039696281
hsa-miR-16-5p	down	-2.744	0.040483415
hsa-miR-21-3p	down	-2.6023	0.044230295
hsa-miR-503-5p	down	-3.7004	0.045651874
hsa-miR-708-3p	down	-2.6778	0.045749055
hsa-miR-340-5p	down	-2.7774	0.045959679
hsa-miR-431-3p	down	-2.9384	0.047335885

Table 3. Dysregulated miRNAs of patient YSX

miRNA_ID	Up/Down (CAF/NF)	Log_2(fold change)	P Value
hsa-miR-144-3p	down	-4.7953	0.000180606
hsa-miR-193b-3p	down	-7.4572	0.000530405
hsa-miR-337-5p	down	-3.5631	0.000880555
hsa-miR-92a-1-5p	up	6.7498	0.001006409
hsa-miR-656-3p	down	-3.2924	0.001353057
hsa-miR-1306-3p	up	2.4626	0.002547333
hsa-miR-205-5p	up	2.5408	0.003567541
hsa-miR-4755-5p	down	-4.4439	0.004066437
hsa-miR-16-2-3p	down	-2.6079	0.005284924
hsa-miR-548av-5p	down	-3.582	0.005759502
hsa-miR-32-5p	down	-2.7547	0.006750367
hsa-miR-200b-5p	up	1.3679	0.009541561
hsa-miR-615-3p	up	1.1862	0.01127765
hsa-miR-4448	up	1.499	0.012795416
hsa-miR-3168	down	-4.0288	0.014145884
hsa-miR-136-3p	down	-2.2889	0.016326336
hsa-let-7i-3p	down	-2.807	0.017699623
hsa-miR-539-3p	down	-2.6531	0.017985498
hsa-miR-29a-3p	down	-2.2277	0.018157726
hsa-miR-942-5p	down	-3.2381	0.019112419
hsa-miR-29b-3p	down	-2.9804	0.019614958
hsa-miR-4683	down	-3.9294	0.019786881
hsa-miR-378b	down	-2.9298	0.023710684
hsa-miR-221-5p	down	-2.21	0.023881327
hsa-miR-223-5p	up	1.3105	0.02695136
hsa-miR-101-3p	down	-2.131	0.027529738
hsa-miR-582-3p	down	-2.3069	0.029363168
hsa-miR-378d	down	-2.1058	0.032239818
hsa-miR-424-5p	down	-2.1225	0.037599892
hsa-miR-655-3p	down	-2.3703	0.038919942
hsa-miR-3182	down	-2.0653	0.045127361
hsa-miR-412-5p	up	1.578	0.049335813
hsa-miR-34c-5p	down	-2.3354	0.049741613

Table 4. Interaction of ten selected genes with upstream miRNAs and downstream genes

miRNAs	miRNA count	Targeted genes	Genes interacted	Gene count	Sum
hsa-miR-10a-3p hsa-miR-29a-3p	2	IGF1	CCND1,FOS	2	4
hsa-miR-29a-3p hsa-miR-34c-5p	2	MYCN	CCND1,PTEN	2	4
hsa-miR-16-5p hsa-miR-424-5p	2	AGO4	CDK6,DICER1	2	4
hsa-miR-10a-3p hsa-miR-16-5p	2	CDC27	CCND1,CDKN1B,CBX2	3	5
hsa-miR-29a-3p hsa-miR-656-3p	2	CCND2	CCND1,CDKN1B,CDK6	3	5
hsa-miR-29a-3p hsa-miR-490-5p	2	FOS	CCND1,CDKN1B,IGF1, PTEN,NFE2L2	5	7
hsa-miR-19b-3p hsa-miR-29a-3p hsa-miR-32-5p	3	PTEN	CCND1,CDKN1B,MYCN, FOS,SYNJ1	5	8
hsa-miR-2682-5p hsa-miR-29a-3p hsa-miR-34c-5p	3	CDK6	CCND1,CDKN1B,CCND2, AGO4,CCNK,WEE1	6	9
hsa-miR-34c-5p hsa-miR-452-5p	2	CDKN1B	CCND1,CCND2,CDK6, FOS,YWHAZ,PTEN,CDC27	7	9
hsa-miR-193b-3p hsa-miR-424-5p	2	CCND1	CDKN1B,CCND2,CDK6, MYCN,BTG2,IGF1,FOS, PTEN,TLE1,CDC27	10	12

Figures

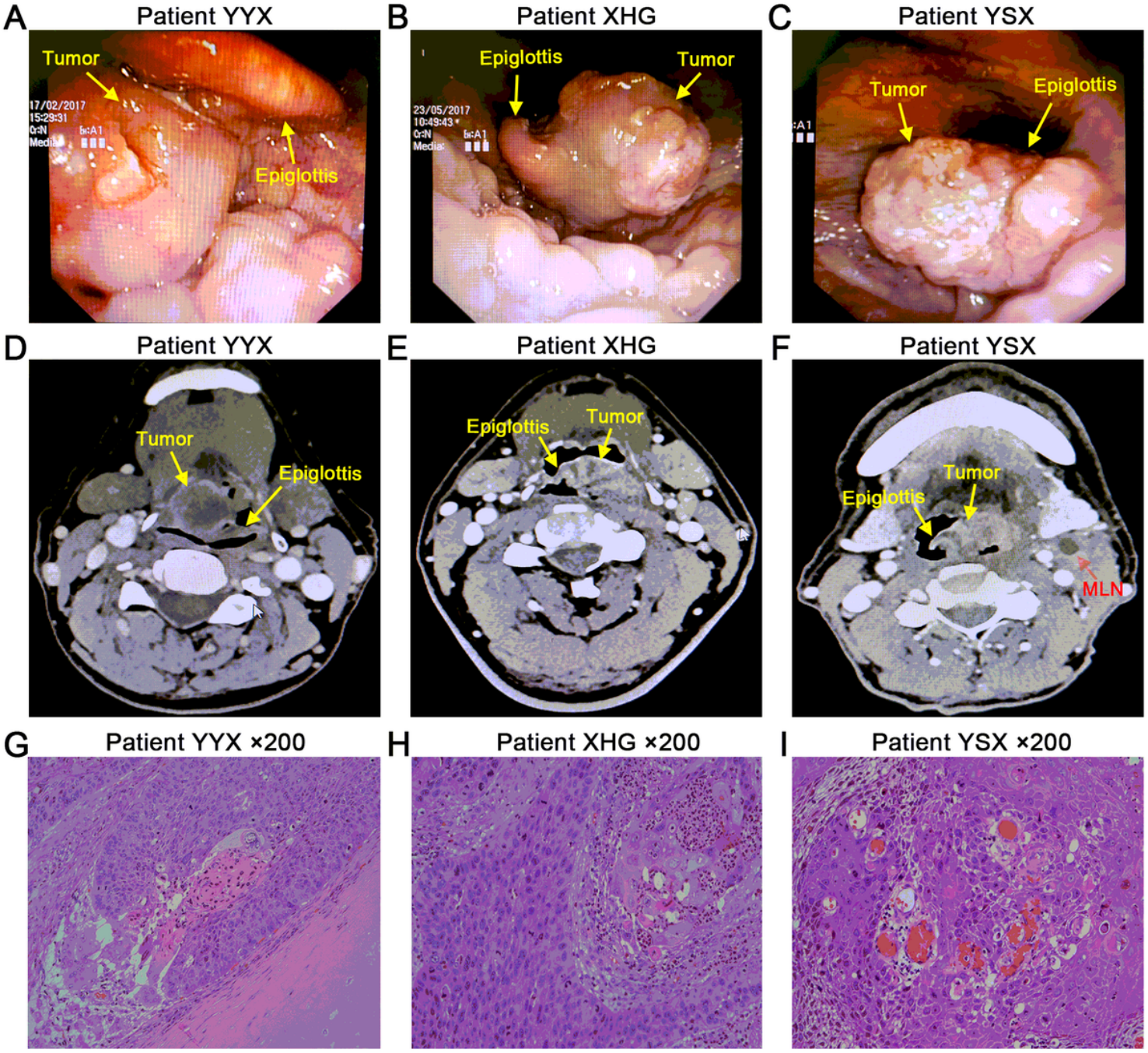

Figure 1

Laryngoscopy, contrast-enhanced CT and pathology of tumours from patients with SLSCC. Typical laryngoscopic photos of tumours from patients (a) YYX, (b) XHG and (c) YSX. All the tumours in three patients originated from the epiglottis. Typical CT images of tumours from patients (d) YYX, (e) XHG and (f) YSX. An obvious metastatic lymph node (MLN) with liquefactive necrosis was observed in the left neck near the submandibular gland in patient YSX. Typical pathological images of tumours from patients (g) YYX, (h) XHG and (i) YSX. All three tumours were moderately differentiated squamous cell carcinomas.

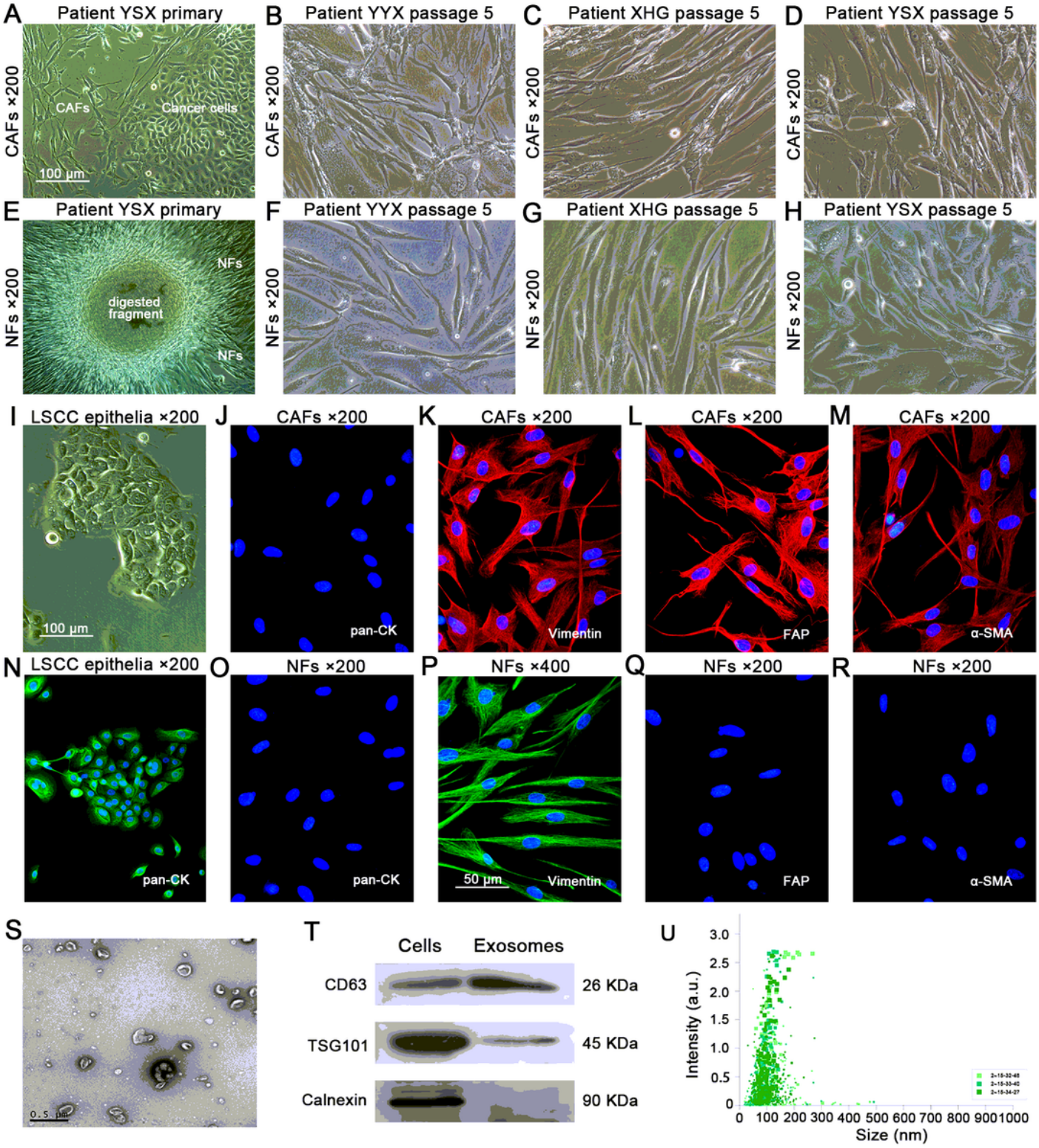

Figure 2

Morphology and immunofluorescence of CAFs and NFs and identification of exosomes. a Primary CAFs co-existed with cancer cells. b-d Purified CAFs at passage 5 from 3 patients. e Primary NFs grew out from the collagenase-digested fragments. f-h Purified paired NFs at passage 5; the NFs showed fewer cell prominences compared to the CAFs. i Morphology of LSCC epithelia. j-m CAFs showed negative staining for pan-CK and positive staining for vimentin, FAP and α-SMA. n Positive control of pan-CK. o-r NFs

showed negative staining for pan-CK, FAP and α-SMA and positive staining for vimentin. s-u TEM images, western blots and NTA data for exosomes.

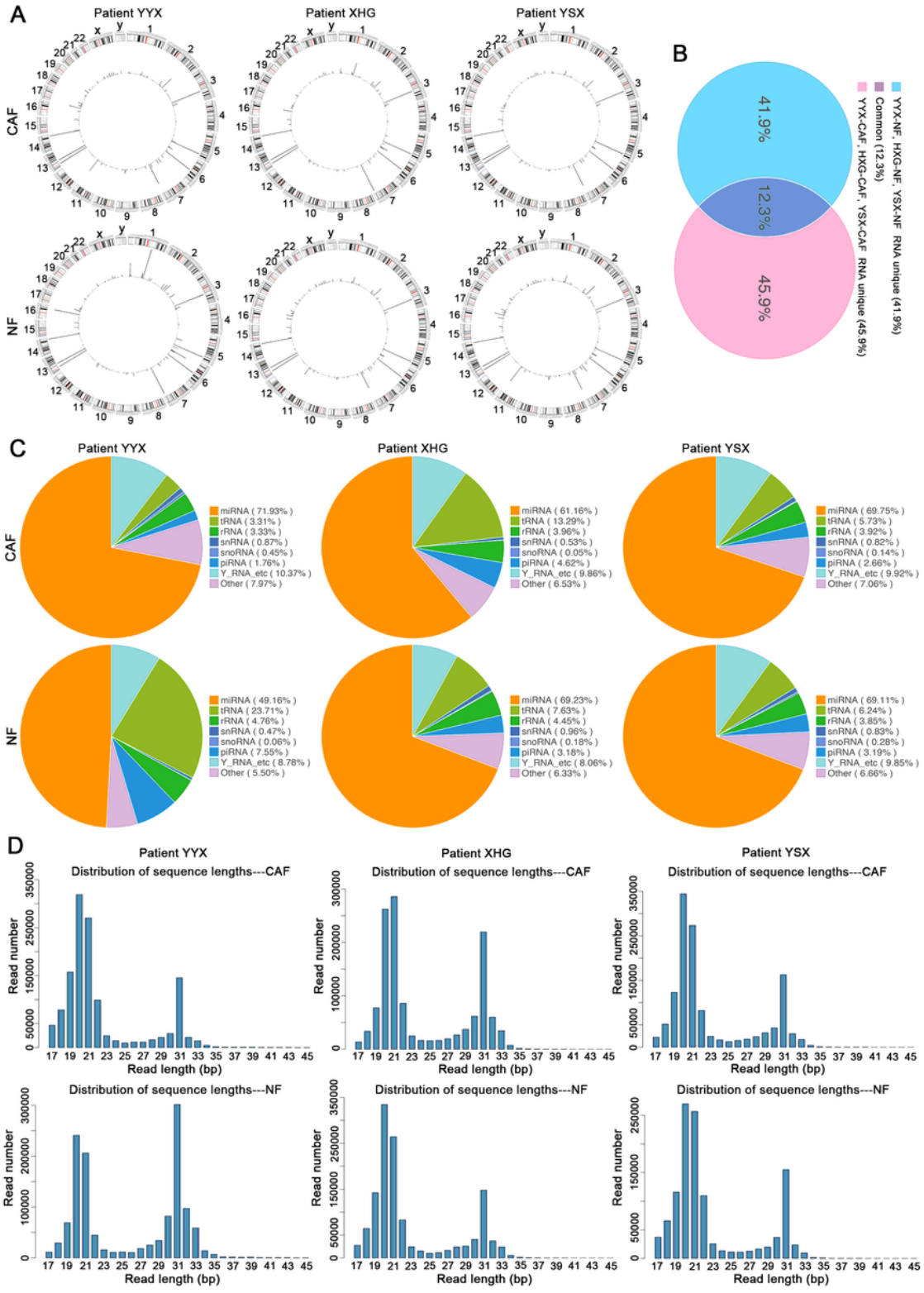

Figure 3

Different small RNA signatures of the exosome compartments and distribution of sequence lengths. a Sample read distribution in the whole genome illustrated by circos plots. The outer ring displays the ID of each chromosome, and the inner ring shows the abundance of RNA in the chromosomal region. The

small RNAs mainly originated from chromosomes 3, 5, 6, 7, 13 and 14. b Illustration of common and unique sequence data in exosomes. c Distributions of small RNA categories in exosomes, illustrated as pie charts. The main identified RNAs in the total small RNA distributions are miRNAs, tRNAs, rRNAs, snRNAs and snoRNAs. d Distribution of sequence lengths of exosomal RNAs. Most sequenced small RNAs were approximately 20 nt and 31 nt (clean reads) in size.

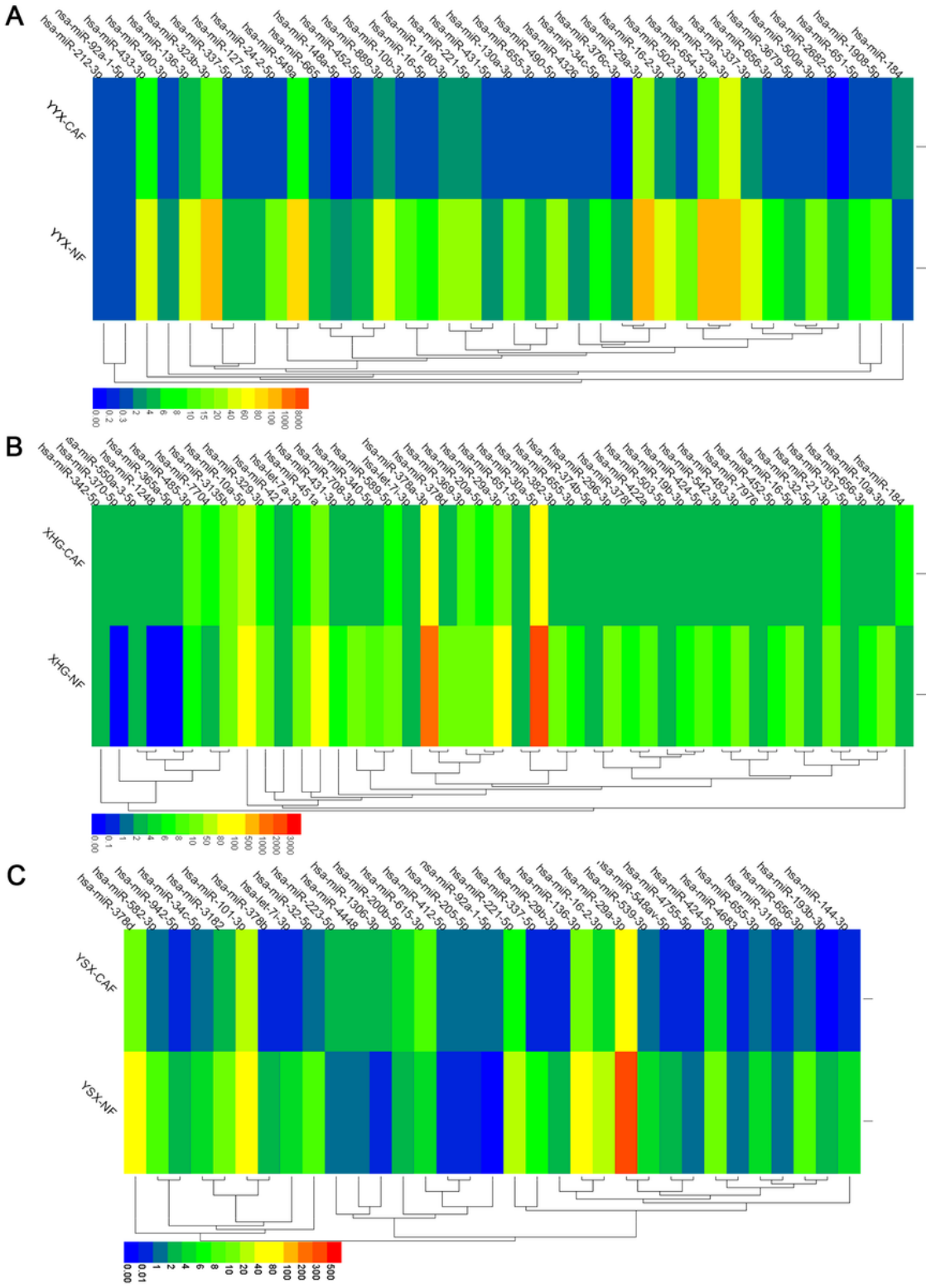

Figure 4

Dysregulated expression profiles of exosomal miRNAs between CAFs and NFs (CAF/NF) illustrated by heat maps. The fold change of log2 served as an inclusion criteria in either direction. Red signal: relative high expression; blue signal: relative low expression. a Patient YYX had 3 miRNAs that were upregulated and the other 42 were downregulated. b Patient XHG had 9 miRNAs that were upregulated and 36 that were downregulated. c Patient YSX had 8 miRNAs that were upregulated and 25 that were downregulated ($P<0.05$).

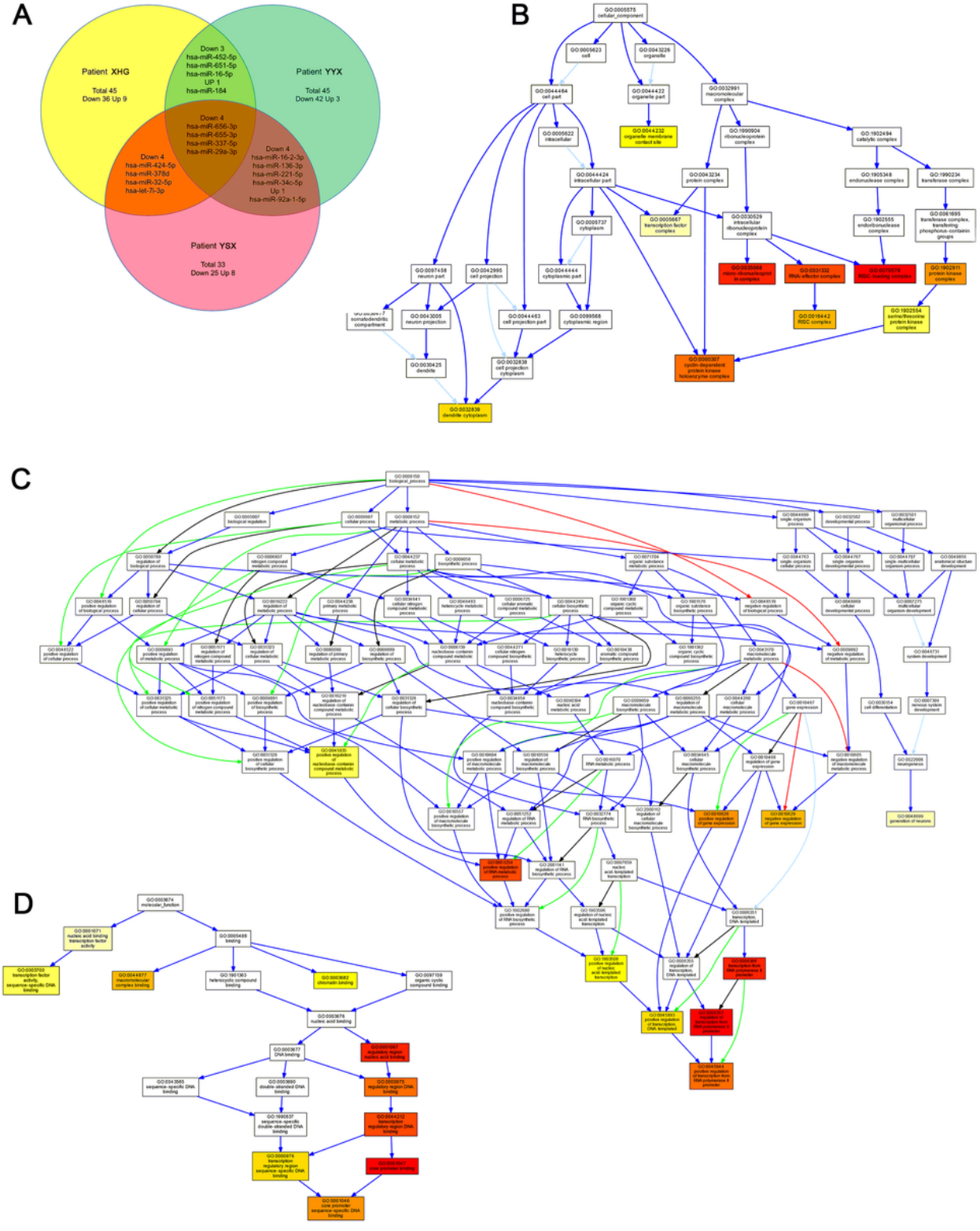

Figure 5

Illustration of dysregulated exosomal miRNAs from three patients with SLSCC and GO annotation of predicted targets. a Three miRNAs were downregulated and 1 miRNA was upregulated in both patient XHG and patient YYX; Four miRNAs were downregulated in both patient XHG and patient YSX; Four miRNAs were downregulated and1 miRNA was upregulated in both patient YSX and patient YYX. Four miRNAs were downregulated simultaneously in all three patients. b-d The GO terms were involved in 3 categories: biological process, cellular component and molecular function (P<0.05).

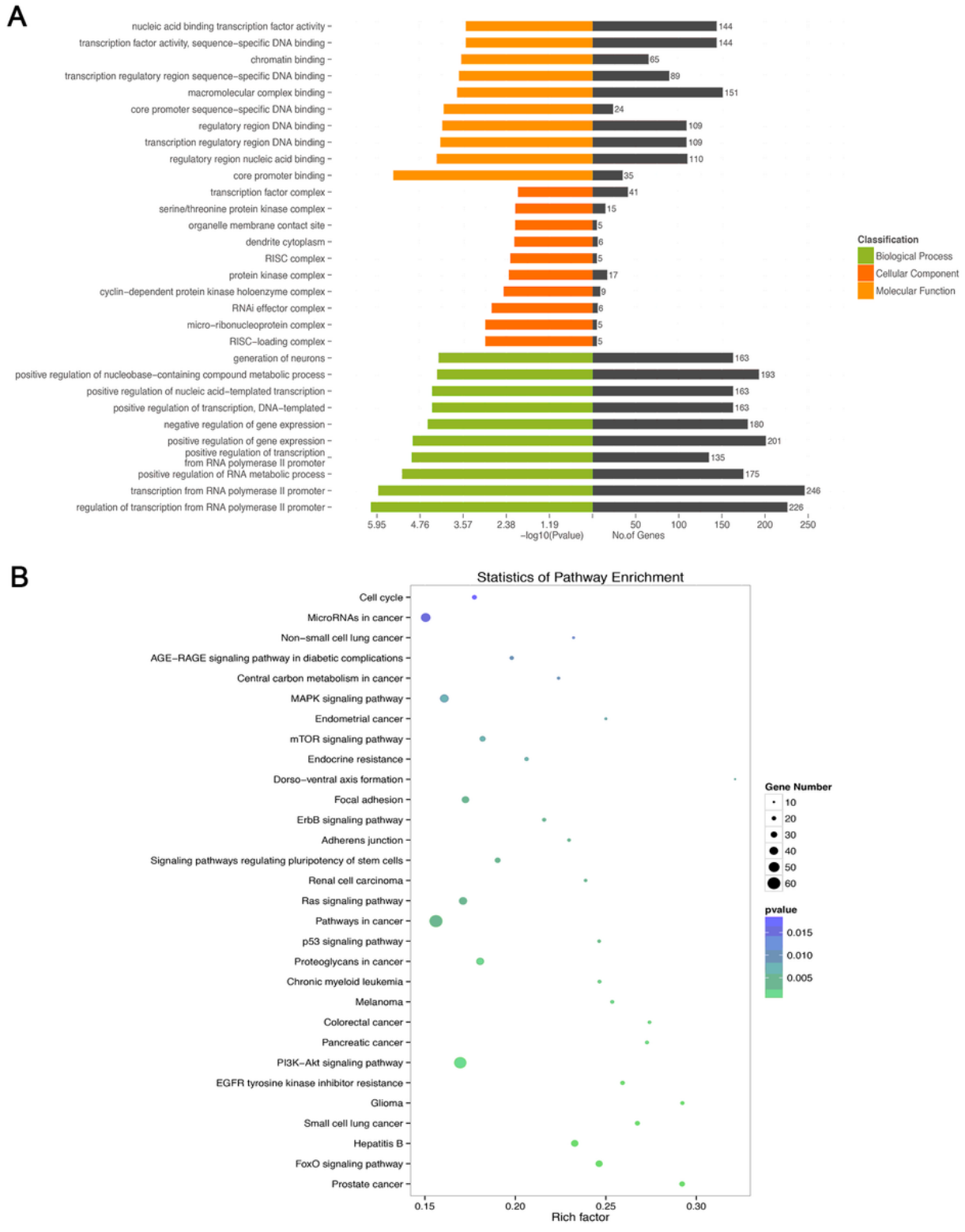

Figure 6

The top ten GO terms in three categories and KEGG pathway enrichment analysis. a The top 10 GO terms are illustrated for the three GO categories (biological process, cellular component and molecular function) (P<0.05). b Thirty signal pathways with greatest statistical differences were selected for the KEGG analysis (P<0.05).

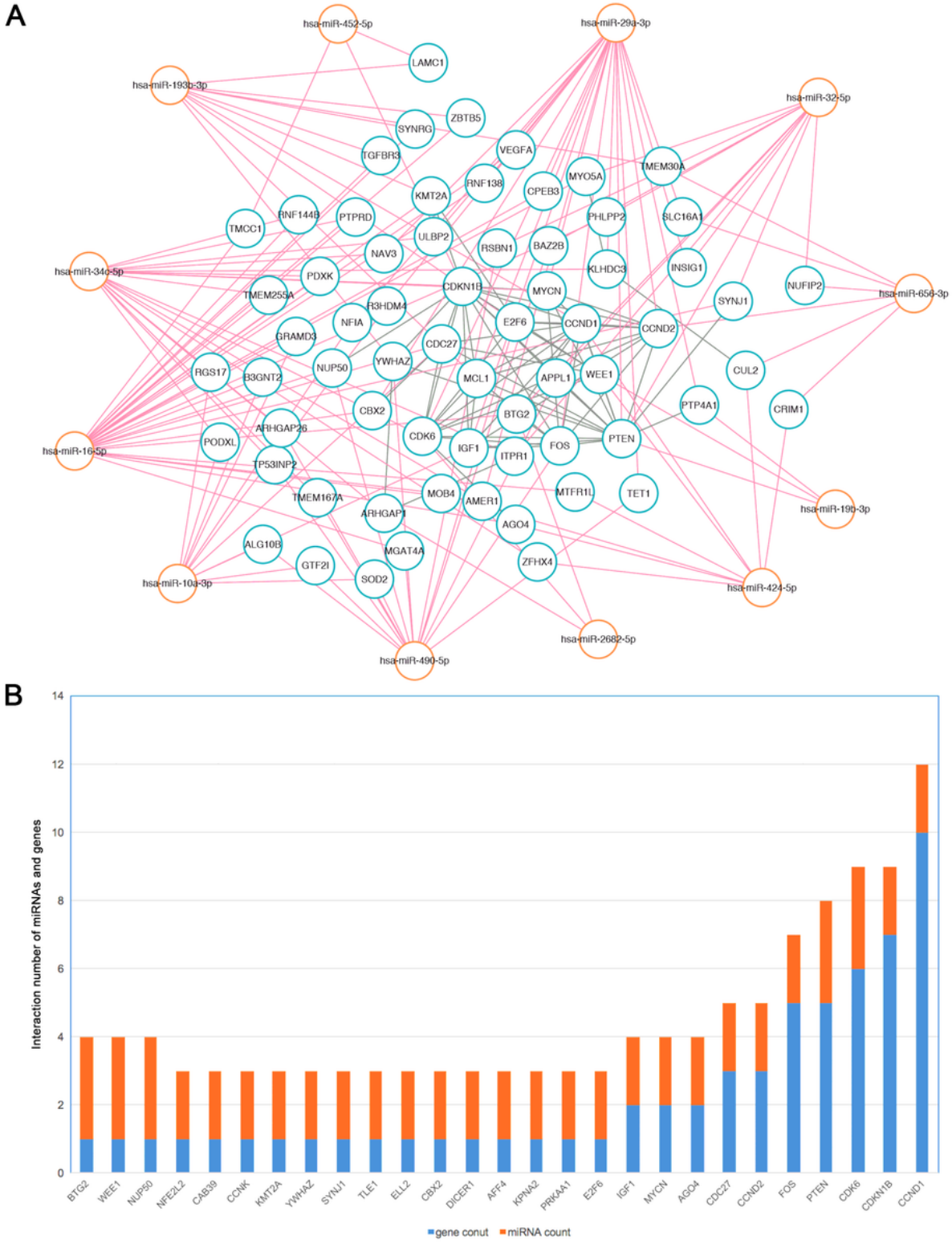

Figure 7

Interaction network of exosomal miRNAs and target genes. a The network revealed the interactions between 12 selected exosomal miRNAs and target genes determined by Cytoscape. b The interaction number of the selected genes with upstream miRNAs and downstream target genes. The orange bars represent the number of upstream miRNAs that regulate the present gene (such as CCND1, 2 upstream miRNAs). The blue bars indicate the number of downstream target genes that interacted with the present gene (such as CCND1, 10 downstream target genes).